

Learning to Calibrate Quantum Control Pulses by Iterative Deconvolution

Xi Cao,^{1,†} Bing Chu,² Haijin Ding,¹ Luyan Sun,³ Yu-xi Liu^{4,5} and Rebing Wu^{1,4,*}

¹*Department of Automation, Tsinghua University, Beijing 100084, China*

²*School of Electronic and Computer Science, University of Southampton, Southampton SO17 1BJ, United Kingdom*

³*Center for Quantum Information, Institute for Interdisciplinary Information Sciences, Tsinghua University, Beijing 100084, China*

⁴*Center for Quantum Information Science and Technology, BNRist, Beijing 100084, China*

⁵*Institute of Micro-Nano Electronics, Tsinghua University, Beijing 100084, China*

In experimental control of quantum systems, the precision is often hindered by the imperfection of applied electronics that distort control pulses delivered to the target quantum devices. To mitigate such error, the deconvolution is commonly used for compensating the distortion via an identified convolutional model, and its effectiveness is limited by the model imprecision (e.g., parameter error or unmodeled nonlinear distortion). In this paper, we propose an iterative scheme that calibrates the pulse by repeatedly applying the deconvolution operation to the error signal. Numerical simulations show that the resulting iterative deconvolution method can correct both linear and nonlinear model errors to an arbitrary precision at the sampling times. Moreover, we find that residue errors between the sampling points are invisible and hence not correctible by iterative deconvolution, but it can be suppressed by actively introducing nonlinear components in the control transmission line.

I. INTRODUCTION

During the past decades, the revolution of quantum information is ongoing [1]. Towards practical applications, high precision control of quantum states and gates operation is a key enabling technology [2, 3]. So far, high-fidelity quantum gates above error-correction threshold have been feasible [4], but there is still a long way to go for scalable quantum computation. The major obstacles include decoherence induced by environmental interactions and systematic errors induced by imperfect control electronics. In particular, systematic errors can be caused by the distortion of control pulses delivered to the qubits [5–12]. For the example of superconducting qubits shown in Fig. 1, the arbitrary waveform generator (AWG) sends control signals to the superconductor quantum circuits via the transmission line [13]. Along the transmission line and associated electronic components, there are linear distortion induced by inductance, capacitors and resonators, as well as nonlinear distortion induced by current-dependent inductances and resistances [5–9, 14, 15]. Besides, in low-temperature experiments, the change of electronic properties of the circuit elements may lead to additional distortions [10, 11]. All these factors can severely degrade the precision of states and gate manipulations and hence

must be corrected.

To compensate the pulse distortion, one can incorporate its model into the optimization process for control pulses design [5]. Alternatively, one can also directly calibrate the pulse according to a designed shape, e.g., the deconvolution method that has been applied to the flux bias control of superconducting quantum circuits [16–18]. In both approaches, a prescribed model is required for characterizing the pulse distortion, and its imprecision limits how much the distortion can be compensated.

Learning from classical control engineering, we propose that the imprecise model can be iteratively used for calibrating pulse to higher precision by learning from errors [19, 20]. The so-called iteration learning control (ILC) has been widely used in processes that can be repeated, such as industrial robots [21, 22], computer numerical control machine tools [23] and autonomous vehicles [24]. In quantum domain, the earliest application of ILC was in the control of chemical reactions with ultrafast laser pulses [25], and it was later on extended to various fields including quantum information processing [26–28]. It should be noted that most quantum ILC applications took the quantum system as a black-box and hence is usually inefficient. This is very different with classical ILC, which takes the system as a grey box (i.e., using an imprecise model) in the learning process to improve the efficiency.

In this paper, we show that the idea of gray-box learning in classical ILC can be applied to quantum systems. As a typical application, we combine the ILC

*rbwu@tsinghua.edu.cn

†zuozhu24@outlook.com

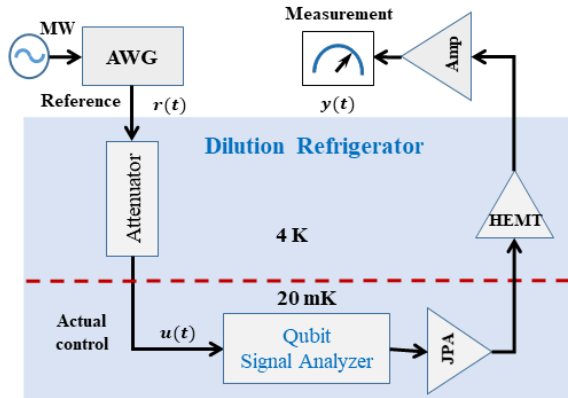


Fig 1: The transmission process of input signals. The reference signal $r(t)$ generated by AWG is distorted when being delivered through the transmission line to the target placed in the refrigerator. The *in situ* signal $u(t)$ is readout from $y(t)$.

and the model used for (offline) deconvolution to calibrate the input signal distortion, which leads to our proposed iterative deconvolution method. The rest of the paper is organized as follows. Section II will summarize the idea of deconvolution, following which the iterative learning deconvolution is proposed. In section III, we show the effectiveness of iterative deconvolution by numerical simulations, as well as its limitation posed by the inter-sampling oscillation induced by finite sampling rate. Section IV studies how the nonlinearity in the distortion can be actively used for suppressing the inter-sampling oscillation. Finally, Section V draws the conclusion.

II. BASIC IDEAS OF ITERATIVE DECONVOLUTION

In this section, we will introduce the deconvolution method and show how it can be improved by iterative learning.

A. Deconvolution

Suppose that we wish to find a proper AWG signal $r(t)$ that produces a desired *in situ* control signal $u_d(t)$ to the quantum system, which cannot be achieved by directly setting $r(t) = u_d(t)$, because the yielded output pulse $u(t)$ will be distorted by the control trans-

mission line that goes from room temperature to the low temperature.

The idea of deconvolution is to identify a linear convolutional input-output model:

$$u(t) = \int_0^\infty \bar{g}(t - \tau)r(\tau)d\tau \quad (1)$$

for the distortion of the desired $r(t)$. In Laplace domain, the convolutional model can be described by transfer function as:

$$u(s) = \bar{G}(s)r(s), \quad (2)$$

where $r(s)$, $u(s)$ and $\bar{G}(s)$ are the Laplace transform of $r(t)$, $u(t)$ and $\bar{g}(t)$. For illustration, we assume that the real dynamics of the distortion is also linear, and is represented by $G(s)$. Then, by setting the reference signal $r(s) = \bar{G}^{-1}(s)u_d(s)$, the produced *in situ* control signal is $u(s) = G(s)\bar{G}^{-1}(s)u_d(s)$. Apparently, when the identified model is precise, i.e., $G(s) = \bar{G}(s)$, the desired signal can be perfectly produced. This inverse-system based method for compensating convolutional distortion is called deconvolution.

B. From deconvolution to iterative deconvolution

In practice, the model $\bar{G}(s)$ is never accurate, due to either imprecise parameters or unmodeled linear or nonlinear dynamics. The errors induced by imprecision model cannot be corrected by the deconvolution method itself, but can be further calibrated in an iterative fashion by repeatedly using the identified model and online data.

Suppose that the *in situ* signal $u(t)$ can be precisely measured from the measured signal $y(t)$, which is another complicated story but will not be discussed here [29]. Denote the initial reference signal by $r^{(0)}(t)$, and the distorted input signal by $u^{(0)}(s) = G(s)r^{(0)}(s)$. We can obtain the error $e^{(0)}(t) = u_d(t) - u^{(0)}(t)$. Then we can modify the reference signal using the error signal and the reference model $\bar{G}(s)$, as follows

$$r^{(1)}(s) = r^{(0)}(s) + \beta\bar{G}^{-1}(s)e^{(0)}(s), \quad (3)$$

where β is the learning rate that needs to be sufficiently small for the stability of the iteration. The updated reference signal is then imposed to the system, following which the error can be obtained for the next iteration of calibration. Inductively, we can repeat this process by updating the reference with

the error signal until the iteration converges. The iterative application of deconvolution compensation is called iterative deconvolution.

According to Eq. (3), it is easy to derive that:

$$e^{(k+1)}(s) = [I - \beta G(s)\bar{G}^{-1}(s)] e^{(k)}(s). \quad (4)$$

Therefore, if one can manage to keep the operator norm $\|I - \beta G(s)\bar{G}^{-1}(s)\|$ smaller than 1, the iterative deconvolution method will guide the reference input to

$$r(s) = G^{-1}(s)u_d(s) \quad (5)$$

that perfectly yields *in situ* signal $u(t) = u_d(t)$. The convergence holds when β is sufficiently small and when the model error is not large (i.e., $G(s)\bar{G}^{-1}(s)$ is reasonably close to identity) [30]. Moreover, as long as the iteration converges, the chosen reference model only affects the rate of convergence, but not on final yield (5). Therefore, the iterative deconvolution is by nature immune to the model imprecision.

III. SIMULATION RESULTS

In this section, we will demonstrate the effectiveness of iterative deconvolution by numerical simulations and analyze the influence of finite sampling time. As shown in Fig. 2, we will simulate the actual signal generation process, in which the AWG produces piecewise control signals after sampling the desired signal, which is followed by linear and nonlinear distortions. In the simulations, we choose the step function as the desired signal, which is more challenging than other smooth signals. Such signals are often required for fast quantum switches [12].

A. Iterative correction of pulse distortion

For illustration, we assume that the real system is described by the following transfer function:

$$G(s) = \frac{1}{(0.008s + 1)(0.001s + 1)}, \quad (6)$$

which involves a slow part (characterized by $T_1 = 0.008$) and a fast part (characterized by $T_2 = 0.001$). We start the test with the following “good” model:

$$\bar{G}_1(s) = \frac{1}{(0.006s + 1)(0.001s + 1)}, \quad (7)$$

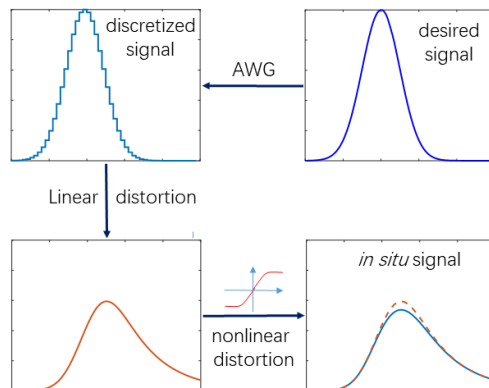


Fig 2: Schematic illustration of the pulse distortion with linear and nonlinear components.

in which only T_1 is slightly different, and the “bad” model:

$$\bar{G}_2(s) = \frac{1}{0.004s + 1}, \quad (8)$$

in which not only T_1 is imprecise, but also the fast dynamics is ignored. We simulate the iteration deconvolution for 100 iterations with sampling period $\tau = 0.002$ (a.u.) and learning rate $\beta = 0.5$, as shown in Fig. 3. It can be clearly seen the iterative deconvolution takes the *in situ* signal from a slowly rising signal shape to a stationary shape that is much closer to the desired step function, no matter which reference model is used, and the same reference input $r(t)$ is obtained. The only difference between using good and bad models is the shape of signal during the intermediate iterations (see the dash red curves). The iteration converges more slowly when using the bad model, but not so much, than that based on the good model. Figure 3 also shows the calibration results with non-iterative deconvolution, under which the performance is much worse. Moreover, the performance of non-iterative calibration is heavily dependent on the accuracy of the reference model, which cannot even achieve desired steady-state value. Therefore, the iterative deconvolution method can effectively improve the performance of deconvolution.

It should be noted that iterative deconvolution may fail when the model is too bad, in which case the iteration diverges. In particular, the iteration is more likely unstable when the distortion dynamics is non-minimum phase, which means that the transfer function contains zeros or poles with positive real parts [31]. In Fig. 4, we simulate the calibration process using the following two non-minimum phase reference

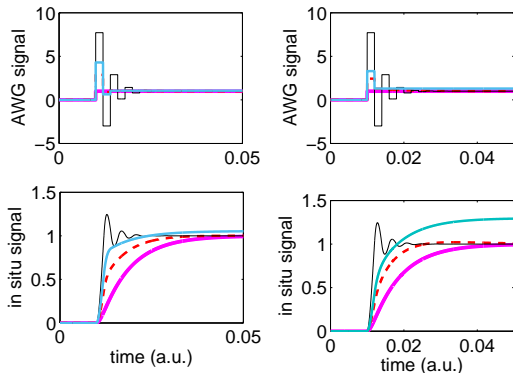


Fig 3: The AWG signals and *in situ* signals using the good model $\bar{G}_1(s)$ and the bad model $\bar{G}_2(s)$, where the AWG sampling period is $\tau = 0.002$ (a.u.). The AWG signal is initially chosen as a step function (purple) and the final yield (after 100 iterations) are shown in black. The dash red curves correspond to the intermediate results (in the 2nd iteration) and the blue curves are obtained by using non-iterative deconvolution.

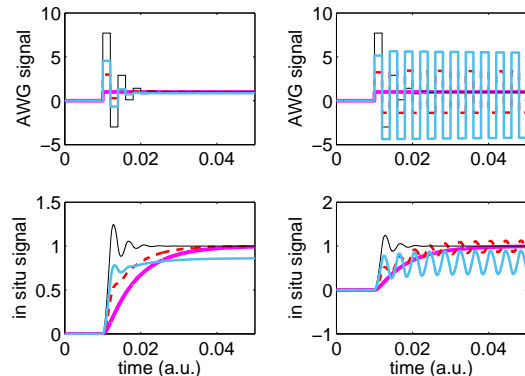


Fig 4: The AWG signals and *in situ* signals using non-minimum-phase models $\bar{G}_3(s)$ and $\bar{G}_4(s)$, where the AWG sampling period is $\tau = 0.002$ (a.u.). The AWG signal is initially set as a step function (purple) and the final yields (after 100 iterations) are shown in black. The dash red curves correspond to the intermediate results (in the 2nd iteration) and the blue curves are obtained by only using deconvolution.

models:

$$\bar{G}_3(s) = \frac{-0.002s + 1}{(0.006s + 1)(0.001s + 1)}, \quad (9)$$

$$\bar{G}_4(s) = \frac{-0.006s + 1}{(0.006s + 1)(0.001s + 1)} \quad (10)$$

that contain zeros in the right half of complex plane. They yield the same reference input as obtained with $\bar{G}_1(s)$ and $\bar{G}_2(s)$. However, the iterated signal exhibits strong oscillations with $\bar{G}_4(s)$ for many iterations, which shows that the calibration process is close to instability. The iterative can completely lose stability when the zero is even closer to the imaginary axis, which will not be shown here.

The above observation implies that one must be cautious when using a non-minimum phase model. Under such circumstance, the above inverse-system based iterative deconvolution (IMID) often fails, and one can turn to the so called norm-optimal iterative deconvolution (NOID) that is much more stable [32]. The NOID is essentially a combination of inverse model algorithm and gradient-based algorithm, and interested readers are referred to [20] for more details.

B. Error analysis

The above simulations show that iterative deconvolution can well outperform the deconvolution itself. However, the eventual calibrated pulse is never, more or less, precisely the same as the desired. Typically, overshoots and damping oscillations appear at the beginning of the calibrated *in situ* signal, due to the finite AWG sampling rate.

To see its influence, we simulate for comparing the iterative deconvolution process with faster sampling scheme $\tau = 0.001$ (a.u.) in Fig. 5. The iteration also successfully converges, but the transient response is different in that the overshoot is higher, the oscillation persists for more periods. Compared to the bad influences, the rising time becomes smaller with higher sampling frequency, which finally reduces the difference between the *in situ* signal and the desired signal. And when looking at only the sampling times [see Fig. 6(a)], we find that, except at the very beginning time, the calibrated *in situ* signal perfectly matches $u_d(t)$ at every sampling point. In other words, the physically existing overshoots and oscillations is invisible to the sampled-data measurements.

It is not hard to understand how this happens. In the first sampling period, the driving field $r(t)$ attempts to drive the *in situ* signal $u(t)$ from 0 to 1 at the first sampling time point $t = \tau$, which requires a

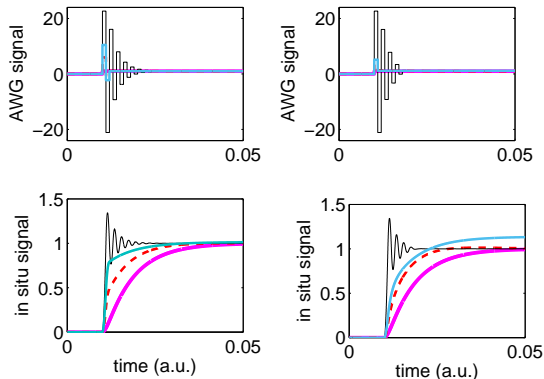


Fig 5: The AWG signals and *in situ* signals using good and bad models (7 and 8), where the AWG sampling period is $\tau = 0.001$ (a.u.). The AWG signal is initially set as a step function (purple) and the final curves (black) after 100 iterations are shown in black. The dash red curves correspond to the intermediate results (in the 2nd iteration) and the blue curves are obtained by only using deconvolution.

high power when the sampling period is short. Due to the inertial dynamics of $G(s)$, $u(t)$ will keep going up after crossing 1 at $t = \tau$. Then, the driving field switches to the opposite direction in order to pull $u(t)$ back to 1 at the second sampling time point $t = 2\tau$, and again the inertia effect brings $u(t)$ down below 1 after $t = 2\tau$. On and on, the inter-sampling oscillations persist and gradually damp. In the Appendix, we prove that no inter-sampling oscillations will occur when $G(s)$ is a first-order system. The inter-sampling behavior is determined by the distortion dynamics $G(s)$, and is independent with the reference model used for calibration. In Figs. 6(c) and 6(d), we show how the highest overshoot and the damping time vary with the time constants T_1 and T_2 for $G(s)$ is described by (A4). It can be clearly seen that the inter-sampling behavior becomes deteriorated for large T_1/τ and T_2/τ , which implies that the calibrated error is small only when the distortion dynamics is as fast as the sampling speed.

Figure 7 shows how the actual and sampled errors, which are defined as follows:

$$\mathcal{E}_{\text{actual}} = \int_0^T |u(t) - u_d(t)| dt, \quad (11)$$

$$\mathcal{E}_{\text{sample}} = \sum_{k=1}^N [u(k\tau) - u_d(k\tau)] \tau. \quad (12)$$

vary in the iteration processes. The sampled error

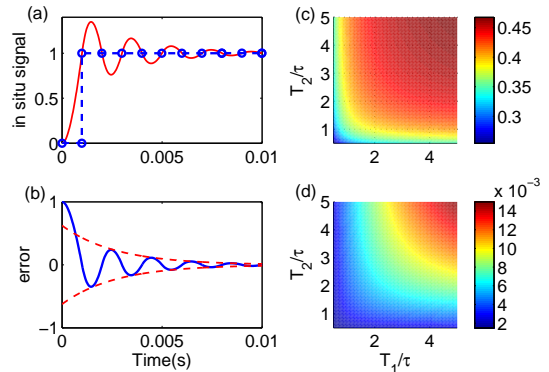


Fig 6: (a). The calibrated *in situ* signal under sampling rate $\tau=0.001$ (a.u.). The signal matches the reference signal perfectly at the sampling points, but is deviated from it in between; (b). The blue curve corresponds to the error between continuous *in situ* signal and the desired in (a), the dashed red lines are Ae^{-t/T_s} and $-Ae^{-t/T_s}$ with the fitted parameters in Eq. (A5); (c). T_s in Eq. (A5) (represent settling time) with different T_1 and T_2 in Eq. (A4); (d). Overshoot with different T_1 and T_2 in Eq. (A4).

can, as expected, be made arbitrarily small, but the actual errors converge to finite values due to the limited sampling rate. Besides, under the same learning rate ($\beta = 0.5$), the convergence is faster when using more precise models. When the model is slightly non-minimum phase, the convergence can be accelerated a little, but this advantage completely loses when the iteration process is close to instability (i.e., when using $\bar{G}_4(s)$ for calibration).

We also plot Fig. 8 to interpret the stability of convergence rate of the iteration from the phase-frequency property of the reference models. As indicated in [30], the iteration is usually stable when the phase difference at the sampling frequency between the reference model and the real model is within 90 degrees (see the area between two dashed line). The convergence becomes faster when the phase of the real model $G(i\omega)$ is in advance of that of the reference model $\bar{G}(i\omega)$. However, the fastness of convergence will lose when the phase of $\bar{G}(i\omega)$ is close to the border of stable region.

IV. ITERATIVE DECONVOLUTION IN PRESENCE OF NONLINEARITY

The above simulations show that iterative deconvolution can effectively improve the performance of

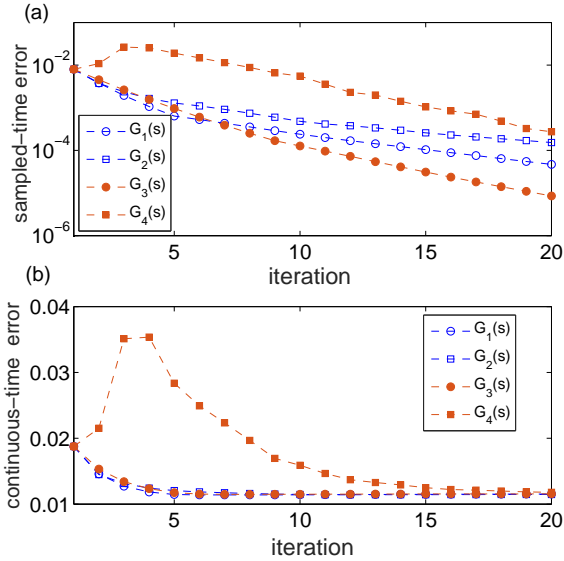


Fig 7: (a). The sampled errors for the iterative deconvolution calibration using models $\bar{G}_1(s)$, $\bar{G}_2(s)$, $\bar{G}_3(s)$ and $\bar{G}_4(s)$; (b). The actual errors for the iterative deconvolution calibration using models $\bar{G}_1(s)$, $\bar{G}_2(s)$, $\bar{G}_3(s)$ and $\bar{G}_4(s)$.

calibration for linear distortion. In this section, we study how the calibration works when there is nonlinearity in the distortion dynamics.

For demonstration, we assume that, after being distorted by $G(s)$, the actual system also experiences the following saturation nonlinearity:

$$S_A(x) = A \tanh\left(\frac{x}{A}\right), \quad (13)$$

where A is the saturation bound. In the simulations shown by Fig. 9, we pick the saturation bound as $A = 2$ and $A = 1$, respectively, and perform the same iterative algorithm using the linear reference model $\bar{G}_1(s)$ for deconvolution. In both cases, the iteration deconvolution can well correct the error, which is achieved when the reference model knows nothing about the nonlinearity. When saturation is relatively small (e.g., when $A = 2$ shown in the figure), and the final calibrated waveform is only slightly different from the case without saturation. More interestingly, when the saturation is properly chosen (i.e., $A = 1$), the final waveform is remarkably different, in a good way, that the inter-sampling overshoots and oscillations are almost completely suppressed. The resulting calibration performance is much better than

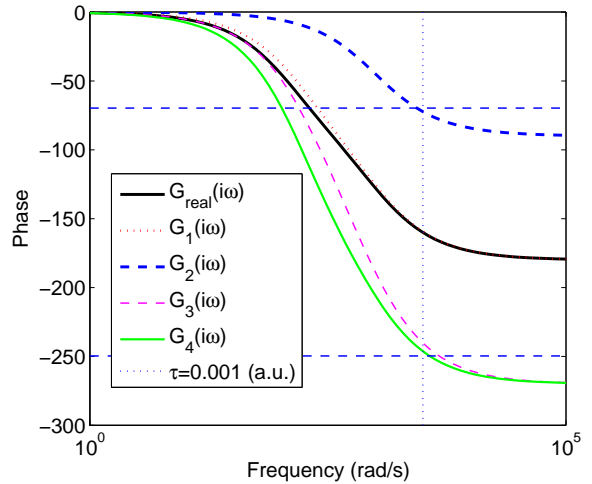


Fig 8: The phase plots for the actual system and the model $\bar{G}_1(s) \sim \bar{G}_4(s)$ used for iterative deconvolution.

the linear case. Therefore, one can actively introduce nonlinearity into the distortion dynamics to improve the calibration performance limited by finite sampling rates.

The saturator introduced above also brings another advantage that the learning process is much more stable, by which one can choose much larger learning rate to accelerate the learning process. As shown in Fig. 10, the learning under the rate $\beta = 0.5$ takes about 300 iterations to reduce the error down to $\mathcal{E}_{\text{actual}} = 10^{-3}$. However, by improving the learning rate to $\beta = 5$, the learning process is still stable and must faster (less than 20 iterations).

V. CONCLUSION

To conclude, we propose that the deconvolution calibration for quantum control pulses can be improved by iterative learning to reduce errors caused by the inaccurate reference model. The simulation results demonstrate that the iterative deconvolution can effectively mitigate the residue error of deconvolution. Moreover, the method is pretty robust to model imprecision and the calibration result is not dependent on the used reference model. We also indicate that the ultimate calibration performance is limited by the inter-sampling oscillations induced by the practically finite sampling rate. The inter-sampling error essentially determined by the *in situ* distortion dynamics,

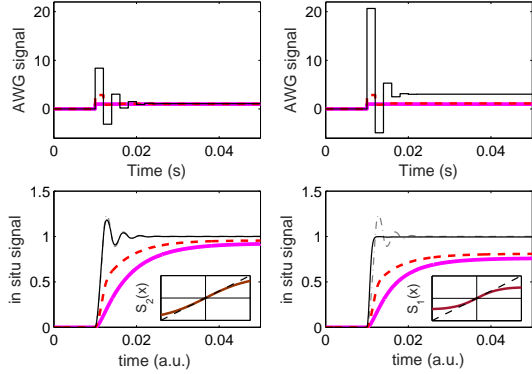


Fig 9: The AWG signals and *in situ* signals using small and large saturation for the model \bar{G}_1 , where the AWG sampling period is $\tau = 0.002$ (a.u.). The AWG signal is initially set as a step function (purple) and the final curves without saturation (dash black) and with saturation (black) after 100 iterations are shown in black. The dash red curves correspond to the intermediate results (in the 2nd iteration).

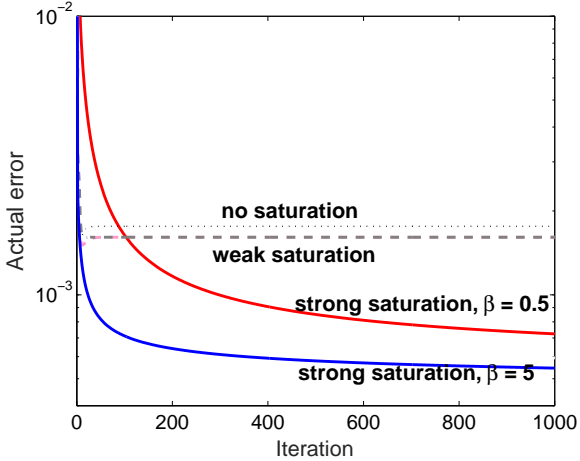


Fig 10: The calibration errors in the iteration process. The active use of saturation nonlinearity can further reduce the calibration error, and one can accelerate the learning process by tuning up the learning rate under which the iteration is still stable.

and cannot be eliminated by the iteration algorithm. However, we show with example that they can be effectively suppressed by proper and active use of non-linearity in the electronic circuits.

Our work exhibits the power of learning by combining imperfect models with online data. Similar ideas

can be applied to many other problems related to quantum control, e.g., quantum process tomography has been proposed for quantum gate tune-up using inaccurate models [12]. For learning quantum control in high-precision regime, this is important that, combined with previous black-box learning methods, the learning process can be much more efficient using *a priori* knowledge from the model that is even not so good, especially when high-quality online measurement data is hard to acquire.

Appendix A: The analysis of inter-sample behavior

For illustration, we assume that the real system is modeled by

$$G(s) = \frac{(\tau_1 s + 1)(\tau_2 s + 1) \cdots (\tau_m s + 1)}{(T_1 s + 1)(T_2 s + 1) \cdots (T_n s + 1)},$$

where $T_1 > T_2 > \cdots > T_n$ and the time constants in the transfer function are not precisely known.

Suppose the required AWG signal is:

$$r(t) = R_1 1(t) + \sum_{k=1}^{\infty} (R_{k+1} - R_k) 1(t - k\tau), \quad (\text{A1})$$

where τ is sampling period and R_n is the magnitude of the signal during the n -th sampling period. Let $h(t)$ be the step response of $G(s)$, then the *in situ* signal $u(t)$ in the first n sampling period can be derived as:

$$u(t, R_1, \dots, R_n) = R_1 h(t) + \sum_{k=1}^{\infty} (R_{k+1} - R_k) h(t - k\tau). \quad (\text{A2})$$

If the desired signal is $u_d(t)$, then (A2) poses n equations for solving R_1, R_2, \dots, R_n as follows:

$$u(\tau, R_1) = u_d(\tau), \quad U(2\tau, R_1, R_2) = u_d(2\tau), \quad \dots \quad (\text{A3})$$

These equations are generally hard to solve. But for first order systems when the desired signal is the step function, it can be easily proven that $R_1 = 1/h(\tau)$ and $R_1 = R_2 = R_3 \dots = R_n$, and the derivation of $u(t)$ after the first sampling point is 0. It implies iterative deconvolution can perfectly correct errors with first-order plants after the first sampling period.

For the second order system:

$$G(s) = \frac{1}{(T_1 s + 1)(T_2 s + 1)}, \quad (\text{A4})$$

we use the function:

$$f(t) = 1 + Ae^{-t/T_s} \sin\left(\frac{2\pi}{T}t\right), \quad (\text{A5})$$

in which T_s corresponds to the damping time of the inter-sampling oscillations (smaller the T_s is, smaller the settling time will be), and A corresponds to the magnitude of overshoot, to present the character of inter-sampling oscillations by fitting the parameters for the simulation data after the first sampling time. Figures 6(b) and 6(c) depict the dependence of the settling time and the overshoot on T_1 and T_2 when $\tau = 0.001$ (a.u.).

-
- [1] M. A. Nielsen and I. L. Chuang, *Quantum computation and quantum information* (Cambridge university press, 2010).
- [2] D. Dong and I. R. Petersen, IET Control Theory A. **4**, 2651 (2010).
- [3] C. Brif, R. Chakrabarti, and H. Rabitz, New J. Phys. **12**, 075008 (2010).
- [4] C. J. Ballance, T. P. Harty, N. M. Linke, M. A. Sepiol, and D. M. Lucas, Phys. Rev. Lett. **117**, 060504 (2016).
- [5] I. N. Hincks, C. E. Granade, T. W. Borneman, and D. G. Cory, Phys. Rev. Applied **4**, 024012 (2015).
- [6] F. Motzoi, J. M. Gambetta, S. T. Merkel, and F. K. Wilhelm, Phys. Rev. A **84**, 022307 (2011).
- [7] P. E. Spindler, Y. Zhang, B. Endeward, N. Gershernzon, T. E. Skinner, S. J. Glaser, and T. F. Prisner, J. Magn. Reson. **218**, 49 (2012).
- [8] S. J. Glaser, U. Boscain, T. Calarco, C. P. Koch, W. Köckenberger, R. Kosloff, I. Kuprov, B. Luy, S. Schirmer, T. Schulte-Herbrüggen, et al., Eur. Phys. J. D **69**, 279 (2015).
- [9] W. Rose, H. Haas, A. Q. Chen, N. Jeon, L. J. Lauhon, D. G. Cory, and R. Budakian, Phys. Rev. X **8**, 011030 (2018).
- [10] R. Patterson, A. Hammoud, and M. Elbuluk, Cryogenics **46**, 231 (2006).
- [11] R. Patterson, A. Hammoud, J. Dickman, S. Gerber, M. Elbuluk, and E. Overton (2004).
- [12] R.-B. Wu, B. Chu, D. H. Owens, and H. Rabitz, Phys. Rev. A **97**, 042122 (2018).
- [13] J. van Dijk, E. Kawakami, R. Schouten, and M. Veldhorst, arXiv:1803.06176v1 (2018).
- [14] H. R. Mohebbi, O. W. B. Benningshof, I. A. J. Taminiau, G. X. Miao, and D. G. Cory, J. Appl. Phys. **115**, 094502 (2014).
- [15] S. A. Maas, *Nonlinear Microwave and RF Circuits* (Artech House Publishers, Boston, MA, 2003).
- [16] B. R. Johnson, *Controlling photons in superconducting electrical circuits* (Yale University, 2011).
- [17] P. A. Jansson, *Deconvolution of images and spectra* (Courier Corporation, 2014).
- [18] P. Bickel, P. Diggle, S. Fienberg, U. Gather, I. Olkin, and S. Zeger, *Deconvolution Problems in Nonparametric* (Springer, 2009).
- [19] D. A. Bristow, M. Tharayil, and A. G. Alleyne, IEEE Control Syst. **26**, 96 (2006).
- [20] D. H. Owens and J. Hätönen, Annu. Rev. Control **29**, 57 (2005).
- [21] S. Arimoto, S. Kawamura, and F. Miyazaki, Proc. IEEE Conf. Decis. Control pp. 1064–1069 (1984).
- [22] M. Norrlof, IEEE Trans. Robot. Autom. **18**, 245 (2002).
- [23] D.-I. Kim and S. Kim, IEEE Trans. Ind. Appl. **32**, 66 (1996).
- [24] Y. Q. Chen and K. L. Moore, Asian J. Control **4**, 90 (2008).
- [25] R. S. Judson and H. Rabitz, Phys. Rev. Lett. **68**, 1500 (1992).
- [26] Y. Long, G. Feng, J. Pearson, and G. Long, Sci. China. Phys. Mech. **57**, 1256 (2014).
- [27] T. Schulte-Herbrüggen, A. Spörl, N. Khaneja, and S. J. Glaser, J. Phys. B: At., Mol. Opt. Phys. **44**, 154013 (2011).
- [28] D. J. Egger and F. K. Wilhelm, Phys. Rev. Lett. **112**, 240503 (2014).
- [29] M. Hofheinz, E. Weig, M. Ansmann, R. C. Bialczak, E. Lucero, A. Neeley, M. and, H. Wang, J. M. Martinis, and A. Cleland, Nature **454**, 310 (2008).
- [30] T. J. Harte, J. Hätönen, and D. Owens, Int. J. Control **78**, 577 (2005).
- [31] G. F. Franklin, J. D. Powell, A. Emami-Naeini, and J. D. Powell, *Feedback control of dynamic systems*,

vol. 3 (Addison-Wesley Reading, MA, 1994).
[32] N. Amann, D. H. Owens, and E. Rogers, IEE. P-

Contr. Theor. Ap. **143**, 217 (1996).